Electronic Supplementary Information

Hierarchically Porous Carbon Materials with Controllable Proportion of Micropore area by Dual-activator Synthesis for High-Performance Supercapacitors

He Xu,[a] ChengkeWu,[a] XianjunWei,[a] Shuyan Gao*[a,b]

[a.]School of Chemistry and Chemical Engineering, Henan Normal University, Xinxiang, Henan 453007, P. R. China.

E-mail: shuyangao@htu.cn; Fax: +86 3733329097; Tel: +86 3733329097

[b.]School of Environment, Henan Normal University, Xinxiang, Henan 453007, P. R. China

Mechanism of KOH activation

It is noteworthy that KOH was used as the activating agent to construct micropores and control the micropores size distributions. During the KOH activation progress, the main products were char, CO, CO_2, H_2O, H_2, K, K_2O and K_2CO_3 at the temperatures under 700°C, and several continuous and/or simultaneous reactions were contained and presented in following Equations (S1)-(S5).[S1,S2] In chemical activation at around 400 °C, K_2O would be generated due to the dehydration of KOH (Equation (1)).[S3] Then H_2 and CO_2 would be produced by the Equations (S2) and (S3). Afterwards, the K_2O and CO_2 can be converted into K_2CO_3 (Equation (S4)).[S1, S4]

$$2KOH \rightarrow K_2O + H_2O \quad \text{(S1)}$$

$$C + H_2O \rightarrow H_2 + CO \quad \text{(S2)}$$

$$CO + H_2O \rightarrow CO_2 + H_2 \quad \text{(S3)}$$

$$CO_2 + K_2O \rightarrow K_2CO_3 \quad \text{(S4)}$$

In addition, the reactions between KOH and carbon materials include solid–solid or solid–liquid processes at about 570 °C that occur by the following stoichiometric redox reaction (Equation (S5)):[S1]

$$6KOH + 2C \rightarrow 2K + 3H_2 + 2K_2CO_3 \quad \text{(S5)}$$

$$K_2CO_3 \rightarrow K_2O + CO_2 \quad \text{(S6)}$$

$$C + K_2O \rightarrow 2K + CO \quad \text{(S7)}$$

Moreover, if the activation temperature achieves over than 700 °C, the as-formed K_2CO_3 (Equation (S4) and (S5)) would transform into CO_2 and K_2O (Equation (S6)), and the K_2O can be further reacted with carbon to form metallic K (Equation (S7)).[S5-S6] It is worth pointing out that metallic K (Equation (S5) and (S7)) can diffuse into the carbon framework efficiently and expands the lattice leading to a rise for the increase of pore volume. Furthermore, in physical activation, the escape of H_2, CO_2, CO and H_2O gas from the biomass carbon can also transform some micropores into mesopores by opening up the closed pores.[S2] After removing the intercalated metallic K and K-containing compounds by the hydrochloric acid washing, the expanded carbon lattices cannot be restored, therefore reasonably generating pores.[S5, S7]

Mechanism of $C_3N_3Na_3S_3$ activation

From the TGA curve of $C_3N_3Na_3S_3$ salt (Fig. S2a), it can be found that the slightly weight loss at 100 ^oC and the obvious weight loss from 600 to 800 ^oC. The slightly weight loss at 100 ^oC may be caused by water evaporation. The obvious weight loss may be owing to the decomposition of $C_3N_3Na_3S_3$when activation temperature was over 600 ^oC. This result were associated with continuous reactions and decomposition of functional groups.[S8-S10]The main products may include char, CO, CO_2, H_2O, H_2, NH_3, and N, O-containing compounds. Therefore the escape of H_2, CO_2, CO, H_2O and NH_3gas from the biomass carbon materials would contribute to the formingof mesopores and macropores.[S11-S13] After removing the metal residue (such as Na^+) by the hydrochloric acid washing, the expanded carbon lattices cannot be restored, therefore reasonably generating pores showing the activated effect.[S14,S15]

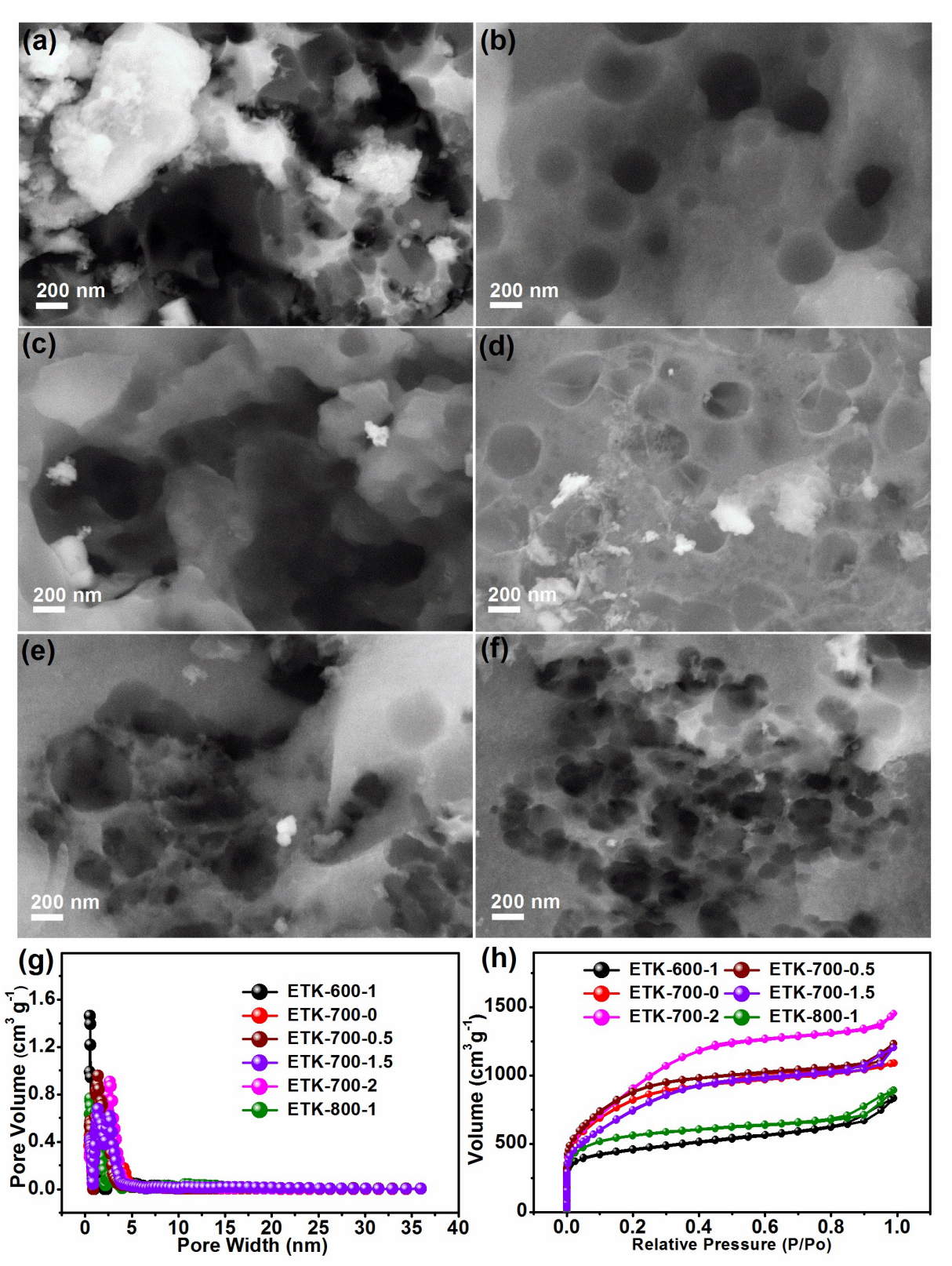

Fig. S1 SEM images of different activated samples: (a) EKT-600-1, (b) ETK-700-0, (c) ETK-700-0.5, (d) ETK-700-1.5, (e) ETK-700-2, and (f) ETK-800-1; (g) pore size distributions of ETK-600-1, ETK-700-0, ETK-700-0.5, ETK-700-1.5, ETK-700-2, ETK-800-1; (h) N_2 adsorption/desorption isotherms of ETK-600-1, ETK-700-0, ETK-700-0.5, ETK-700-1.5, ETK-700-2, ETK-800-1.

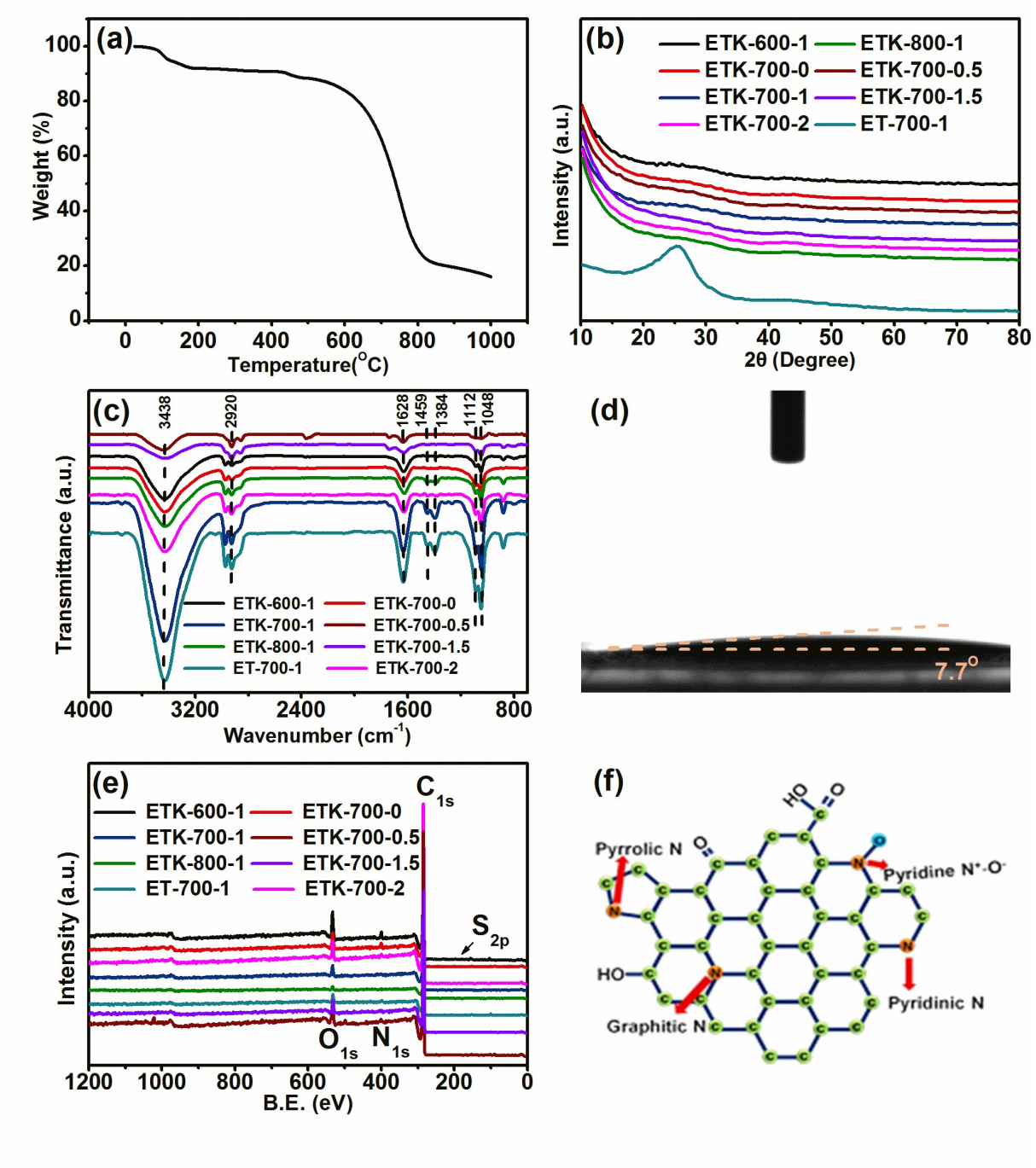

Fig. S2 (a) TGA curve of the $C_3N_3Na_3S_3$salt in N_2 atmosphere, (b) XRD patterns for all samples, (c) FIIR spectra of all samples, (d) contact angle of ETK-700-1, (e) XPS spectra of all samples, (f) schematic model of N-containing and O-containing functional surface groups on carbon.

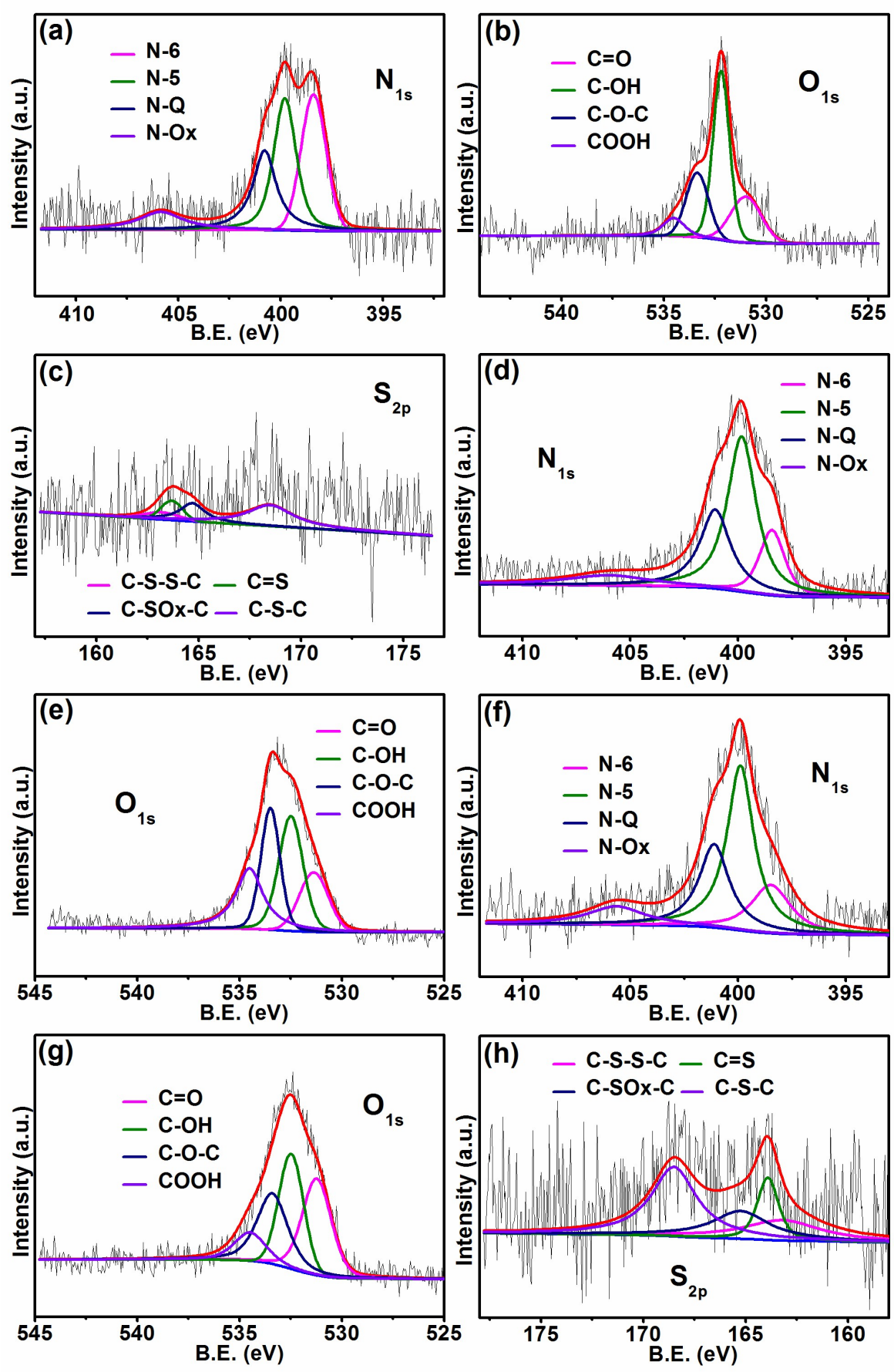
(a)
N-6
N-5
N-Q
N-Ox
N1s
Intensity (a.u.)
410
405
400
395
B.E. (eV)
(b)
C=O
C-OH
C-O-C
COOH
O1s
Intensity (a.u.)
540
535
530
525
B.E. (eV)
(c)
S2p
C-S-S-C
C=S
C-SOx-C
C-S-C
Intensity (a.u.)
160
165
170
175
B.E. (eV)
(d)
N-6
N-5
N-Q
N-Ox
N1s
Intensity (a.u.)
410
405
400
395
B.E. (eV)
(e)
C=O
C-OH
C-O-C
COOH
O1s
Intensity (a.u.)
545
540
535
530
525
B.E. (eV)
(f)
N-6
N-5
N-Q
N-Ox
N1s
Intensity (a.u.)
410
405
400
395
B.E. (eV)
(g)
C=O
C-OH
C-O-C
COOH
O1s
Intensity (a.u.)
545
540
535
530
525
B.E. (eV)
(h)
C-S-S-C
C=S
C-SOx-C
C-S-C
S2p
Intensity (a.u.)
175
170
165
160
B.E. (eV)

Fig. S3 (a) N_{1s}, (b) O_{1s} and (c) S_{2p} high-resolution XPS spectra of ET-700-1 with deconvoluted peaks, (d) N_{1s}, and (e) O_{1s} high-resolution XPS spectra of ETK-600-1 with deconvoluted peaks, (f) N_{1s}, (g) O_{1s} and (h) S_{2p} high-resolution XPS spectra of ETK-700-0 with deconvoluted peaks.

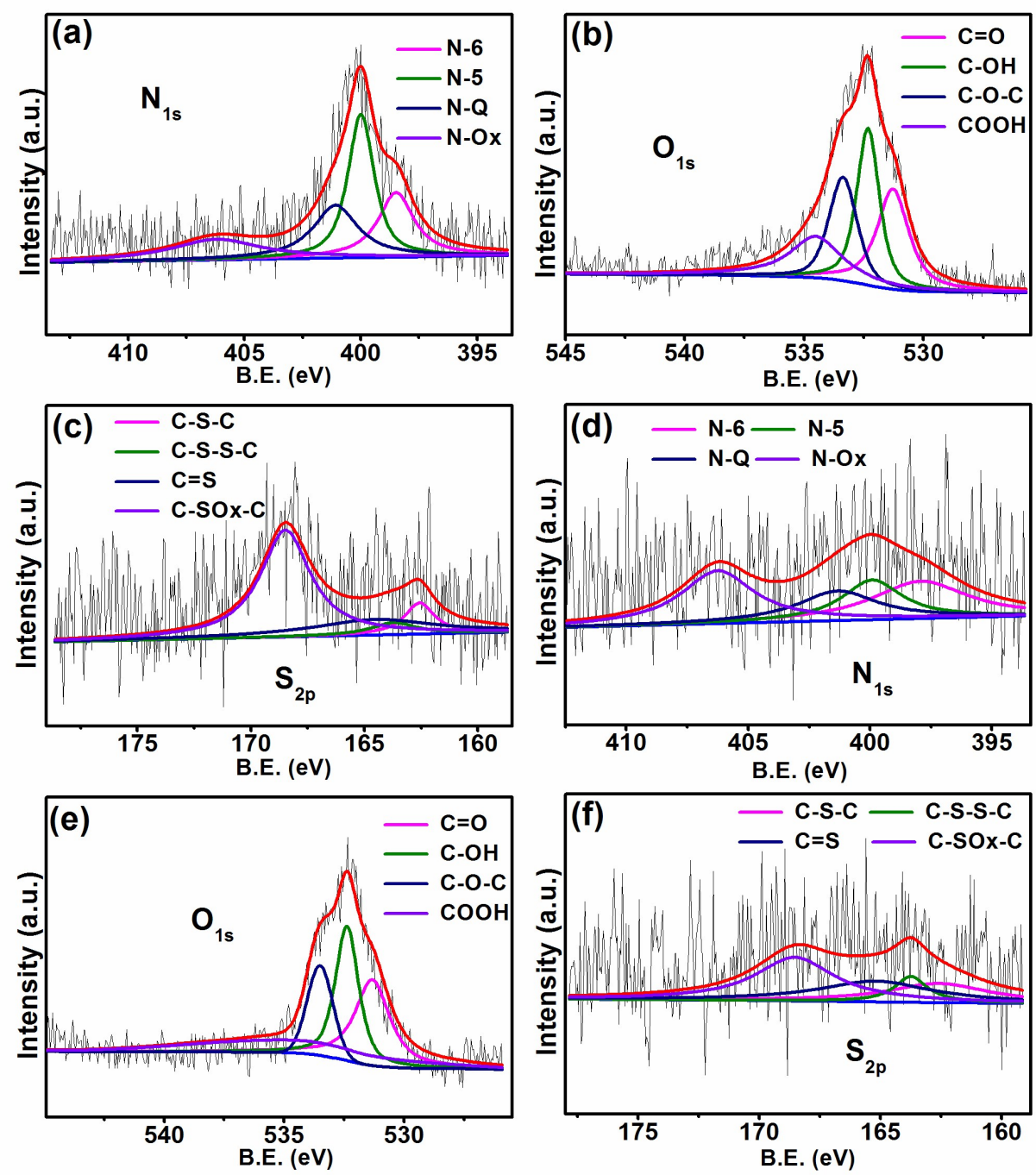

Fig. S4 (a) N_{1s}, (b) O_{1s} and (c) S_{2p} high-resolution XPS spectra of ETK-700-0.5 with deconvoluted peaks, (d) N_{1s}, (e) O_{1s} and (f) S_{2p} high-resolution XPS spectra of ETK-700-1.5 with deconvoluted peaks.

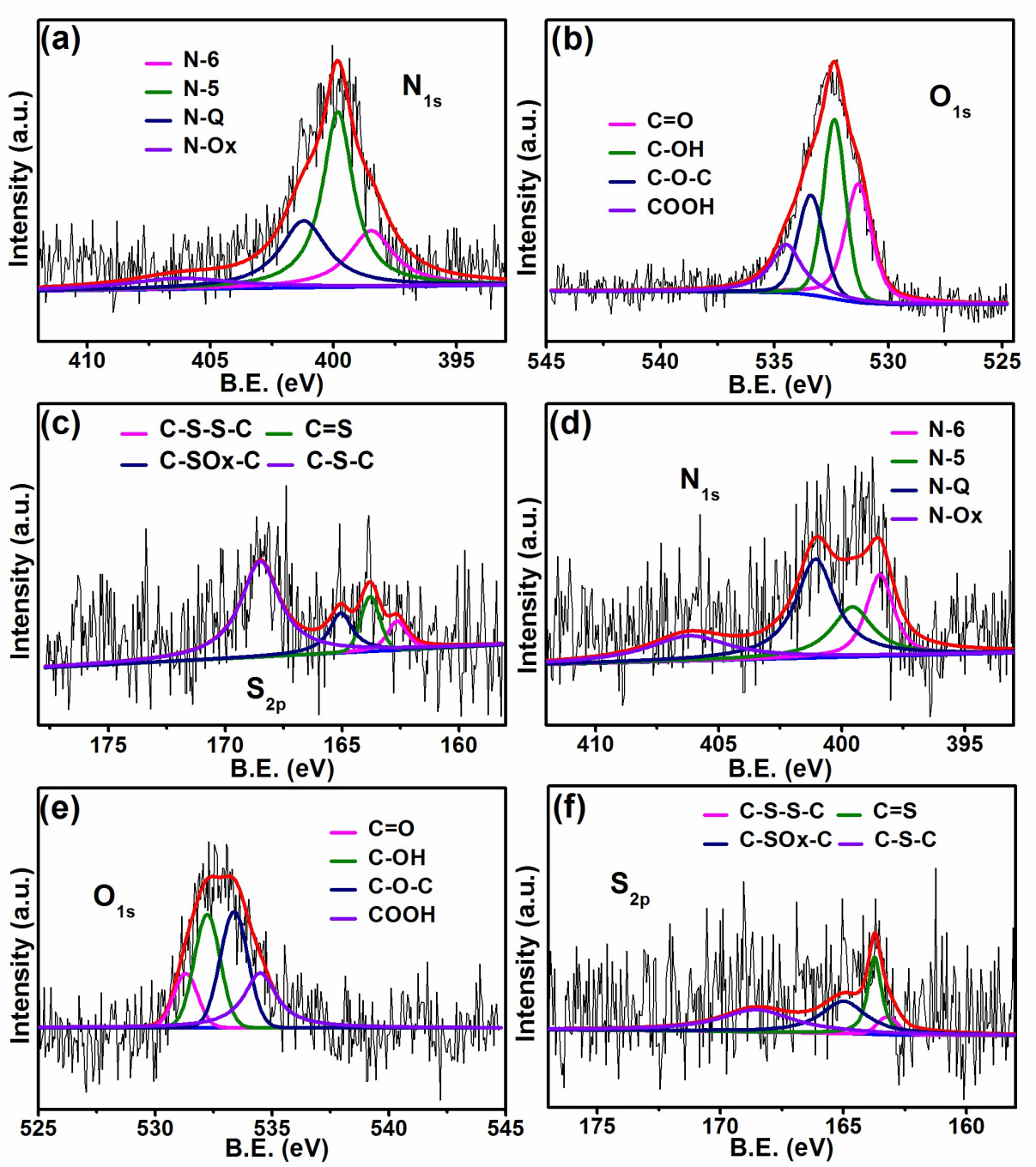

Fig. S5 (a) N_{1s}, (b) O_{1s} and (c) S_{2p} high-resolution XPS spectra of ETK-700-2 with deconvoluted peaks, (d) N_{1s}, and (e) O_{1s} and (f) S_{2p} high-resolution XPS spectra of ETK-800-1 with deconvoluted peaks.

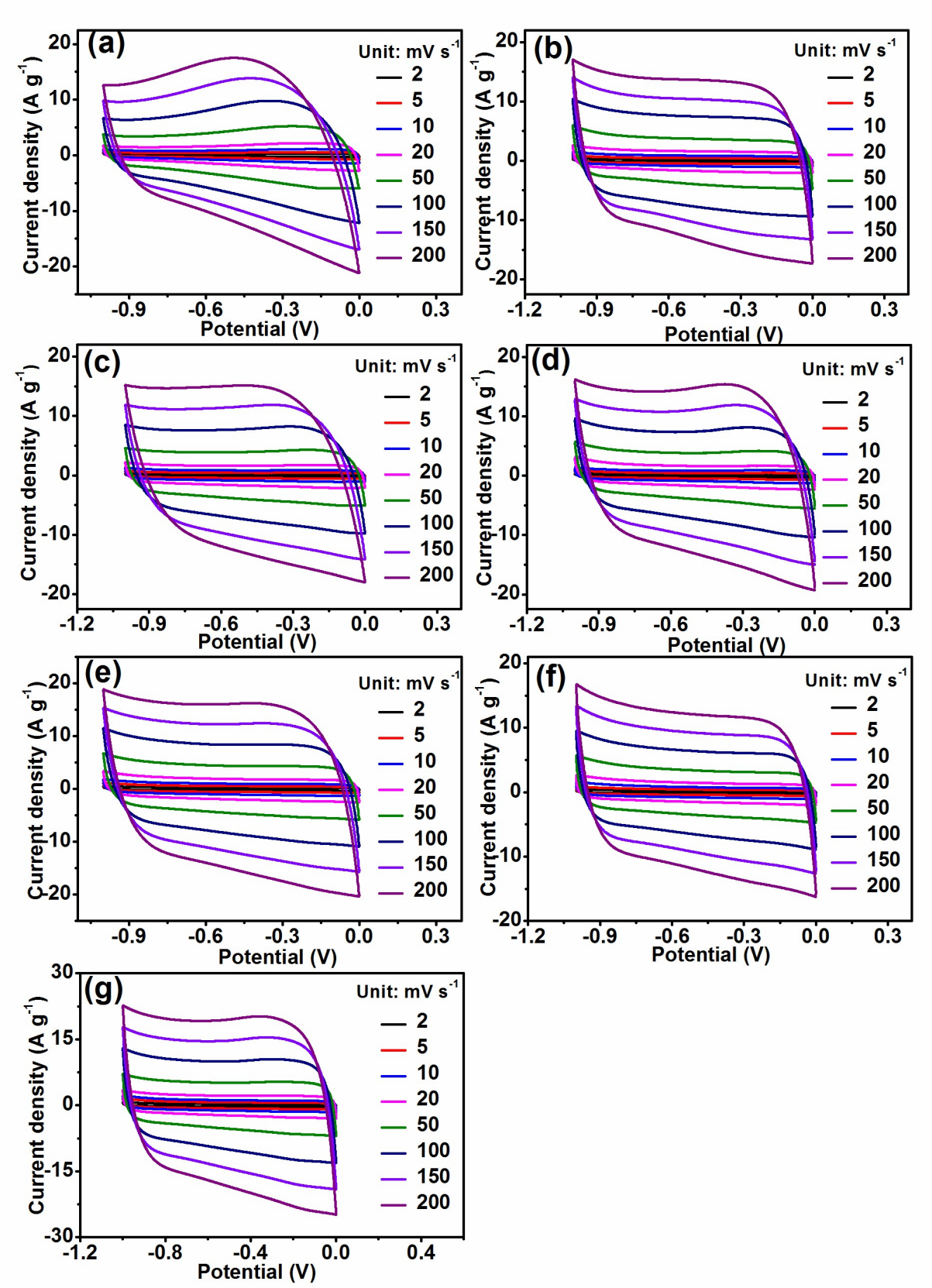

Fig. S6 CV curves of the obtained samples under the different sweep rates: (a) ETK-600-1, (b) ETK-700-0, (c) ETK-700-0.5, (d) ETK-700-1.5, (e) ETK-700-2, (f) ETK-800-1, (g) ETK-700-1.

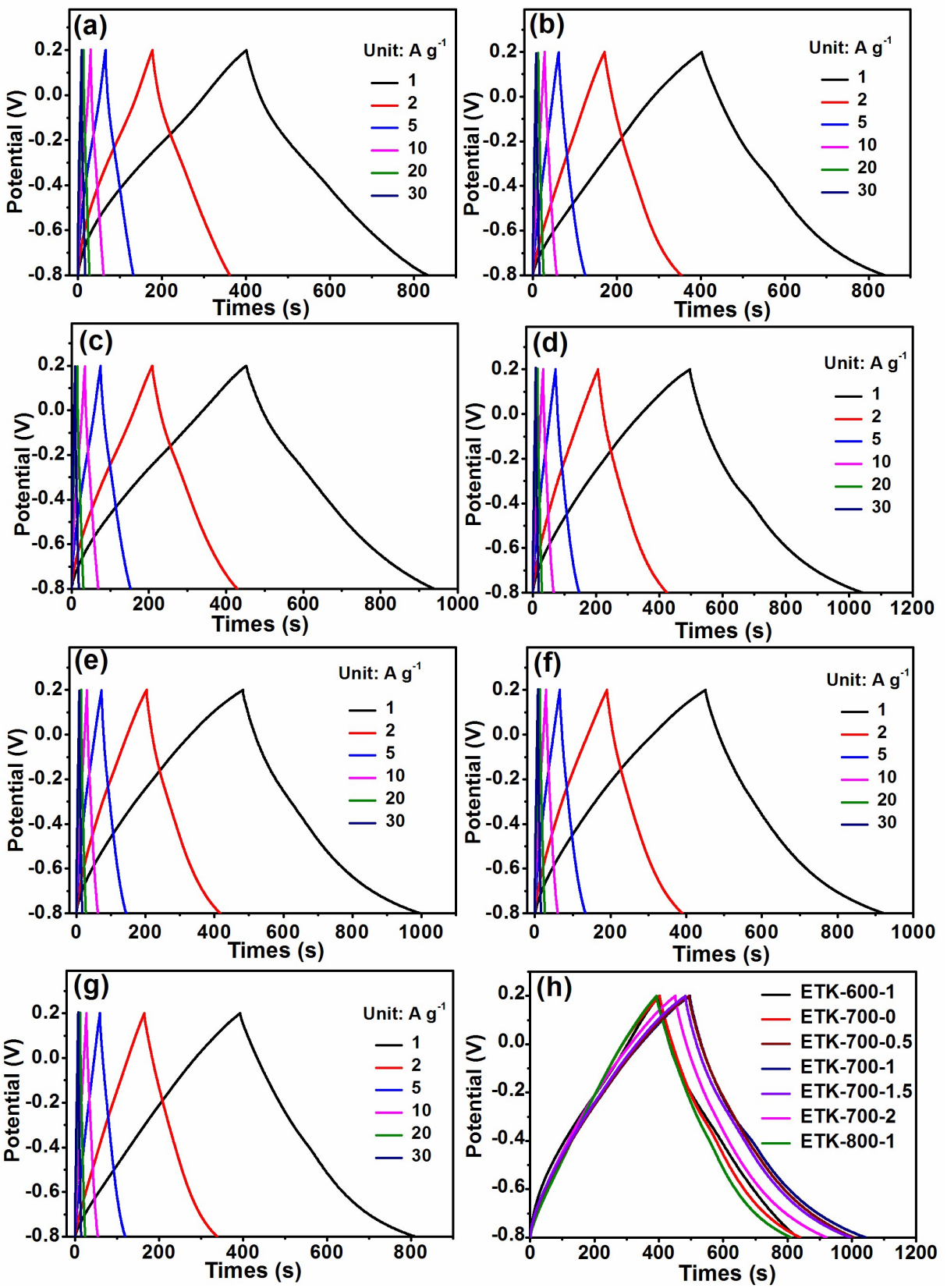

Fig. S7 GCD curves of the obtained samples at various current densities from 1 to 30 A g^{-1} in 1 mol L^{-1} H_2SO_4 electrolyte in the three-electrode system: (a) ETK-600-1, (b) ETK-700-0, (c) ETK-700-0.5, (d) ETK-700-1, (e) ETK-700-1.5, (f) ETK-700-2, (g) ETK-800-1;(h) the GCD curves of the obtained samples at 1 A g^{-1} in 1 mol L^{-1} H_2SO_4 electrolyte in the three-electrode system.

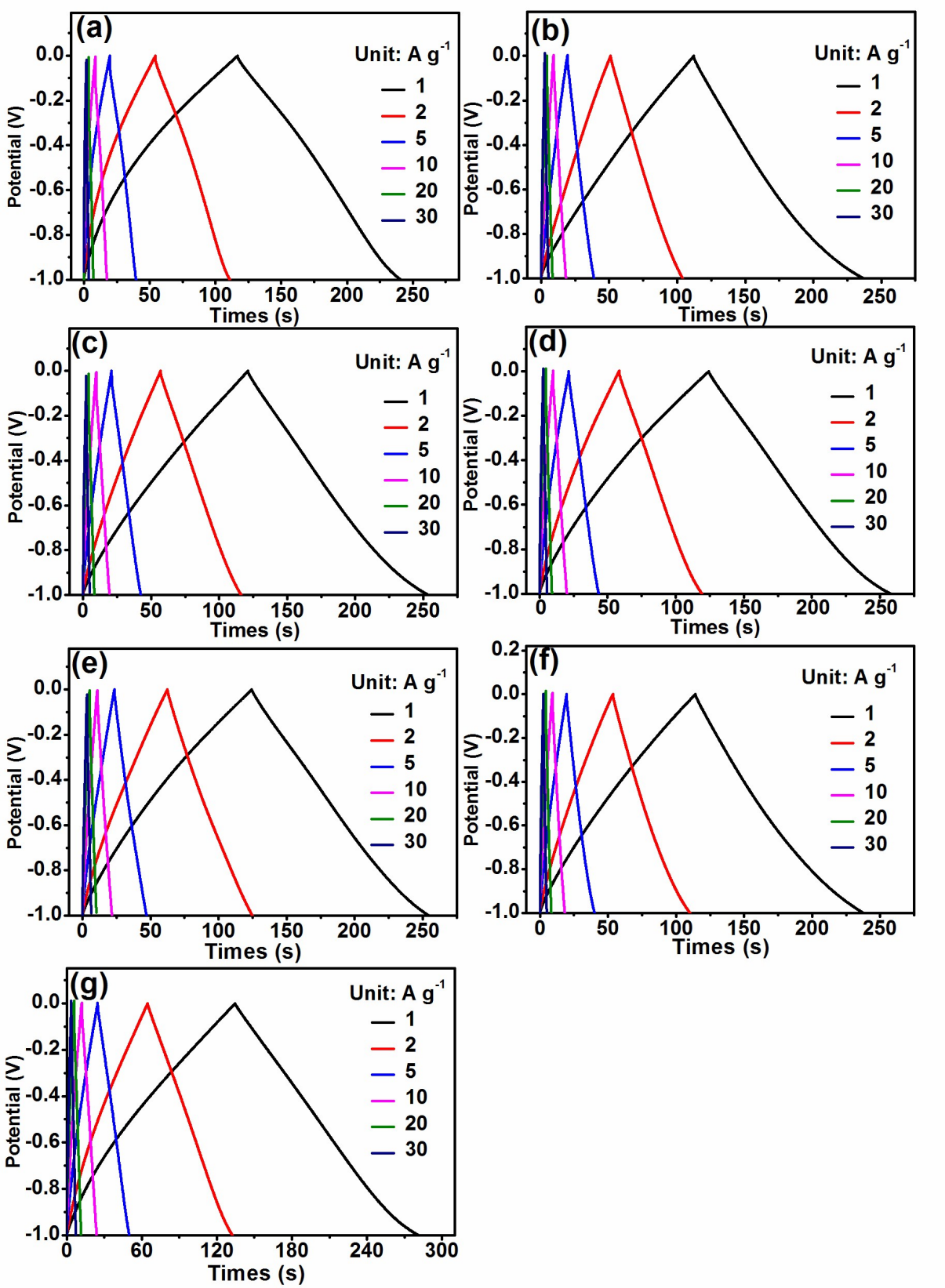

Fig. S8 GCD curves of the obtained samples at various current densities from 1 to 30 A g^{-1} in 1 mol L^{-1} H_2SO_4 electrolyte in the two-electrode system: (a) ETK-600-1, (b) ETK-700-0, (c) ETK-700-0.5, (d) ETK-700-1.5, (e) ETK-700-2, (f) ETK-800-1, and (g) ETK-700-1.

Table S1 Detailed quantitative element analysis data.

Sample	Atomic ratio (%)											
	C_{1s}	O_{1s}	O_{1s}				N_{1s}	N_{1s}				S_{2p}
			C=O	C-OH	C-O-C	COOH		N-6	N-5	N-Q	N-O_x	
ETK-600-1	85.60	10.37	17.76	31.23	25.67	25.34	3.14	15.78	47.37	26.97	9.88	—
ETK-700-0	91.59	6.06	31.58	29.34	27.73	11.35	2.22	18.12	45.24	25.74	10.90	0.12
ETK-700-0.5	94.18	4.13	27.97	29.12	22.47	20.44	1.30	23.09	34.49	23.71	18.71	0.39
ETK-700-1	92.91	5.75	16.45	18.44	21.85	43.26	1.03	4.74	26.37	35.67	33.22	0.32
ETK-700-1.5	96.30	3.54	31.53	30.18	17.37	20.92	0.13	28.52	19.84	19.76	31.88	0.03
ETK-700-2	93.83	4.84	29.72	32.26	21.28	16.74	1.19	20.54	43.96	25.69	9.81	0.14
ETK-800-1	93.72	4.83	12.82	29.01	31.78	26.39	1.43	19.76	20.55	39.17	20.52	0.02
ET-700-1	93.60	4.05	22.19	47.31	22.65	7.85	2.30	30.89	33.31	24.89	10.91	0.05

Table S2 Comparison of electrochemical performances of the carbon materials synthesized from biomass in supercapacitors.

Materials	Surface area [$m^2\ g^{-1}$]	Electrolyte	Capacitance [$F\ g^{-1}$]	E [$Wh\ kg^{-1}$]	P [$kW\ kg^{-1}$]	Reference
Egg yolk	3519	H_2SO_4	549[a; b]	12.7	6.0	This study
Watermelon	—	KOH	333 [a; b]	—	—	[S16]
Chitosan	1582	KOH	252 [a; c]	—	—	[S17]
Cellulose	859	H_2SO_4	328 [a; c]	—	—	[S18]
Cotton	2436	KOH	283 [a; b]	—	—	[S19]
Bagasse	2064	H_2SO_4	142 [a; c]	19.7	0.5	[S20]
Human hair	1306	KOH	340 [a; b]	45.3	2.2	[S21]
Pomelo Peel	2725	KOH	342 [a; e]	9.4	0.1	[S22]
Shiitake Mushroom	2988	KOH	306 [a; b]	8.2	13.0	[S23]
Waste Air-laid Paper	1470	KOH	296 [a; c]	34.3	0.3	[S24]
Waste oily sludge	2561	KOH/PVA gel	348 [a; c]	7.22	0.1	[S25]
Celtuce Leaves	3290	KOH	361 [a; b]	—	—	[S26]
Rice husk	1768	KOH	233 [a; f]	8.36	—	[S27]
Coconut Shell	2440	H_2SO_4	221.4 [a; g]	7.6	4.5	[S28]
RF Resins	2178	KOH	222 [d; c]	10.1	8.0	[S29]
Pomelo Peel	2191	KOH	342 [a; b]	17.1	3.8	[S30]
Fungus	1103	KOH	360 [a; b]	22.0	—	[S31]
NCAs	1626	KOH	354 [a; e]	—	—	[S32]

[(a)] Capacitance with three-electrode system, [(b)]the current density of 1 A g^{-1}, [(c)]the current density of 0.5 A g^{-1}, [(d)]capacitance with two-electrode system, [(e)]the current density of 0.2 A g^{-1}, [(f)]the current density of 2 A g^{-1}, [(g)]the current density of 5 A g^{-1}.

Notes and references

[S1]M. Sevilla, A. B. Fuertes and R. Mokaya, *Energy Environ. Sci.*, 2011, **4**, 1400-1410.

[S2] X. Wei, H. Zou and S. Gao, *Carbon*, 2017, **123**, 471-480.

[S3] L. Qie, W. Chen, H. Xu, X. Xiong, Y. Jiang, F. Zou, X. Hu, Y. Xin, Z. Zhang and Y. Huang, *Energy Environ. Sci.*, 2013, **6**, 2497-2504.

[S4] E. Raymundo-Piñero, P. Azaïs, T. Cacciaguerra, D. Cazorla-Amorós, A. Linares-Solano and F. Béguin, *Carbon,* 2005, **43**, 786-795.

[S5] J. Gañan, C. M. González-Garćıa, J. F. González, E. Sabio, A. Maćıas-Garćıa and M. A. Dıaz-Dıez, *Appl. Surf. Sci.,* 2004, **238**, 347-354.

[S6] Y. Sudaryanto, S. B. Hartono, W. Irawaty, H. Hindarso and S. Ismadji, *Bioresource Technol,* 2006, **97**, 734-739.

[S7] X. Wei, Y. Li and S. Gao, *J. Mater. Chem. A,* 2017, **5**, 181-188.

[S8] T. E. Rufford, D. Hulicova-Jurcakova, K. Khosla, Z. Zhu and G. Q. Lu, *J. Power Sources,* 2010, **195**, 912-918.

[S9] Z. Sun, S. Wang, L. Yan, M. Xiao, D. Han and Y. Meng, *J. Power Sources*, 2016, **324**, 547-555.

[S10] X. Li, X. Cheng, M. Gao, D. Ren, Y. Liu, Z. Guo, C. Shang, L. Sun and H. Pan, *ACS Appl. Mater. Interfaces*, 2017, **9**, 10717-10729.

[S11] X. Wei, H. Zouand S. Gao, *Carbon*, 2017, **123**, 471-480.

[S12] X. Wei, S. Wan and S. Gao, *Nano Energy*, 2016, **28**, 206-215.

[S13] C. Di Blasi, C. Brancaand A. Galgano, *Polym. Degrad. Stab.,* 2008, **93**, 335–346.

[S14] J. Gañan, C. M. González-Garćıa, J. F. González, E. Sabio, A. Maćıas-Garćıa and M. A. Dıaz-Dıez, *Appl. Surf. Sci.,* 2004, **238**, 347-354.

[S15] X. Wei, Y. Li and S. Gao, *J. Mater. Chem. A,* 2017, **5**, 181-188.

[S16]X. L. Wu, T. Wen, H. L. Guo, S. Yang, X. Wang and A. W. Xu, *ACS Nano*, 2013, **7**, 3589-3597.

[S17] X. Deng, B. Zhao, L. Zhu and Z. Shao, *Carbon,* 2015, **93**, 48-58.

[S18]H. Zhuo, Y. Hu, X. Tong, L. Zhong, X. Peng and R. Sun, *Ind. Crops Prod.,* 2016, **87**, 229-235.

[S19]P. Cheng, T. Li, H. Yu, L. Zhi, Z. Liu and Z. Lei, *J. Phys. Chem. C*, 2016, **120**, 2079-2086.

[S20] P. Hao, Z. Zhao, J. Tian, H. Li, Y. Sang, G. Yu, H. Cai, H. Liu, C. P. Wong and A. Umar, *Nanoscale,* 2014, **6**, 12120-12129.

[S21] W. Qian, F. Sun, Y. Xu, L. Qiu, C. Liu, S. Wang and F. Yan, *Energy Environ. Sci.,* 2014, **7**, 379-386.

[S22] Q. Liang, L. Ye, Z. H. Huang, Q. Xu, Y. Bai, F. Kang and Q. H. Yang, *Nanoscale*, 2014, **6**, 13831-13837.

[S23] P. Cheng, S. Gao, P. Zang, X. Yang, Y. Bai, H. Xu, Z. Liu and Z. Lei, *Carbon,* 2015, **93**, 315-324.

[S24] J. Pu, C. Li, L. Tang, T. Li, L. Ling, K. Zhang, Y. Xu, Q. Li and Y. Yao, *Carbon,* 2015, **94**, 650-660.

[S25] X. Li, K. Liu, Z. Liu, Z. Wang, B. Li and D. Zhang, *Electrochim. Acta*, 2017, **240**, 43-52.

[S26] R. Wang, P. Wang, X. Yan, J. Lang, C. Peng and Q. Xue, *ACS Appl. Mat. Interfaces,*2012, **4**, 5800-5806.

[S27] X. He, P. Ling, M. Yu, X. Wang, X. Zhang and M. Zheng, *Electrochim. Acta*, 2013, **105**, 635-641.

[S28] A. Jain, C. Xu, S. Jayaraman, R. Balasubramanian, J. Y. Lee and M. P. Srinivasan, *Microporous Mesoporous Mater.,* 2015, **218**, 55-61.

[S29] H. Xuan, Y. Wang, G. Lin, F. Wang, L. Zhou, X. Dong and Z. Chen, *RSC Adv.,* 2016, **6**, 15313-15319.

[S30] C. Peng, J. Lang, S. Xu and X. Wang, *RSC Adv.,*2014, **4**, 54662-54667.

[S31] C. Long, X. Chen, L. Jiang, L. Zhi and Z. Fan, *Nano Energy*, 2015, **12**, 141-151.

[S32] J. Zhang, G. Chen, Q. Zhang, F. Kang and B. You, *ACS Appl. Mat. Interfaces,* 2015, **7**, 12760-12766.